Human Molecular Genetics, 2016, Vol. 25, No. 3 597–608

doi: 10.1093/hmg/ddv499
Advance Access Publication Date: 8 December 2015
Original Article

ORIGINAL ARTICLE

De novo dominant *ASXL3* mutations alter H2A deubiquitination and transcription in Bainbridge–Ropers syndrome

Anshika Srivastava[1], K.C. Ritesh[1], Yao-Chang Tsan[1], Rosy Liao[1], Fengyun Su[2,3], Xuhong Cao[2,3], Mark C. Hannibal[4], Catherine E. Keegan[1,4], Arul M. Chinnaiyan[2,3], Donna M. Martin[1,4] and Stephanie L. Bielas[1,*]

[1]Department of Human Genetics, [2]Howard Hughes Medical Institute, Department of Pathology, [3]Departments of Urology, Computational Medicine and Bioinformatics, and [4]Department of Pediatrics, University of Michigan Medical School, Ann Arbor, MI, USA

*To whom correspondence should be addressed at: Department of Human Genetics, University of Michigan Medical School, 3703 Medical Science II, 1137 Catherine St. SPC 5618, Ann Arbor, MI 48109-5618, USA. Tel: +1 7346478890; Fax: +1 7347633784; Email: sbielas@umich.edu

Abstract

De novo truncating mutations in *Additional sex combs-like 3 (ASXL3)* have been identified in individuals with Bainbridge–Ropers syndrome (BRS), characterized by failure to thrive, global developmental delay, feeding problems, hypotonia, dysmorphic features, profound speech delays and intellectual disability. We identified three novel *de novo* heterozygous truncating variants distributed across *ASXL3*, outside the original cluster of *ASXL3* mutations previously described for BRS. Primary skin fibroblasts established from a BRS patient were used to investigate the functional impact of pathogenic variants. *ASXL3* mRNA transcripts from the mutated allele are prone to nonsense-mediated decay, and expression of ASXL3 is reduced. We found that ASXL3 interacts with BAP1, a hydrolase that removes mono-ubiquitin from histone H2A lysine 119 (H2AK119Ub1) as a component of the Polycomb repressive deubiquitination (PR-DUB) complex. A significant increase in H2AK119Ub1 was observed in *ASXL3* patient fibroblasts, highlighting an important functional role for ASXL3 in PR-DUB mediated deubiquitination. Transcriptomes of *ASXL3* patient and control fibroblasts were compared to investigate the impact of chromatin changes on transcriptional regulation. Out of 564 significantly differentially expressed genes (DEGs) in *ASXL3* patient fibroblasts, 52% were upregulated and 48% downregulated. DEGs were enriched in molecular processes impacting transcriptional regulation, development and proliferation, consistent with the features of BRS. This is the first single gene disorder linked to defects in deubiquitination of H2AK119Ub1 and suggests an important role for dynamic regulation of H2A mono-ubiquitination in transcriptional regulation and the pathophysiology of BRS.

Introduction

Bainbridge–Ropers syndrome (BRS; OMIM 615485) is characterized by failure to thrive, feeding problems, global developmental delay, hypotonia, intellectual disability (ID) and delays in language acquisition (1). *De novo* dominant truncating mutations in *Additional sex combs-like 3 (ASXL3)* have emerged as the cause of BRS, while missense mutations in *ASXL3* have been identified in individuals with Autism Spectrum Disorder (ASD) (2–4). With massively parallel DNA sequencing, *de novo* heterozygous mutations have emerged as a prominent cause of ASD and ID. A disproportionate fraction of *de novo* mutations disrupt chromatin remodeling genes, implicating epigenetic dysregulation of gene

Received: September 8, 2015. **Revised:** November 5, 2015. **Accepted:** December 1, 2015

transcription as an important molecular mechanism (3,5–7). Here we describe three novel truncating variants in *ASXL3* that extend beyond the original cluster of those previously described. These mutations help to define the genotypic spectrum across *ASXL3* associated with the clinical features of BRS.

ASXL genes are mammalian homologues of drosophila *Additional sex combs* (*Asx*). Members of this gene family enhance transcription regulation by Polycomb-group (PcG) and Trithorax-group (TrxG) complexes (8–10). The ASXL family consists of three members (ASXL1, ASXL2 and ASXL3) that share a common domain architecture: i.e. ASXN, ASXH, ASXM1, ASXM2 domains and a PHD finger (Fig. 1D) (11–13). Germline mutations of *ASXL1* and *ASXL3* occur in patients with congenital disorders, whereas truncating somatic mutations of all three ASXL family members are observed in human cancers (11,14). Many molecular functions have been predicted for ASXL3 based on its similarity to other ASXL family members, yet few have been confirmed. ASXL1 is the most recognized ASXL family member and functions as an epigenetic scaffold for ubiquitin C-terminal hydrolase BAP1, histone lysine methyltransferase EZH2 and nuclear receptors (15). While ASXL1 exhibits a range of scaffolding interactions, both germline and somatic mutations in *ASXL1* have been closely linked to changes in H3K27me3 through its association with EZH2.

A series of in vitro assays were important for characterizing the interaction between ASXL1 and BAP1 to form the human Polycomb repressive deubiquitination (PR-DUB) complex. This complex functions to remove the mono-ubiquitin from lysine 119 of histone H2A (H2AK119Ub1), which is primarily ubiquitinated by Polycomb Repressive complex 1 (PRC1) (16). BAP1 is a ubiquitin carboxy-terminal hydrolase that deubiquitinates H2AK119Ub1 as a component of the PR-DUB complex. PR-DUB formation is critical for normal function, as BAP1 alone does not exhibit H2AK119Ub1 deubiquitination activity. However, while BAP1 is a required component of a PR-DUB, ASXL1 may be interchangeable with other ASXL family members to form an enzymatically active complex (17,18). We used primary dermal fibroblasts established from a BRS patient to investigate the molecular defects underlying truncating mutations in *ASXL3*. *De novo* truncating transcripts are subject to nonsense-mediated decay, negatively impacting overall ASXL3 expression. We show that ASXL3 interacts with BAP1 forming the key components of the PR-DUB complex. This is an important functional interaction as the level of H2AK119Ub1 is significantly increased

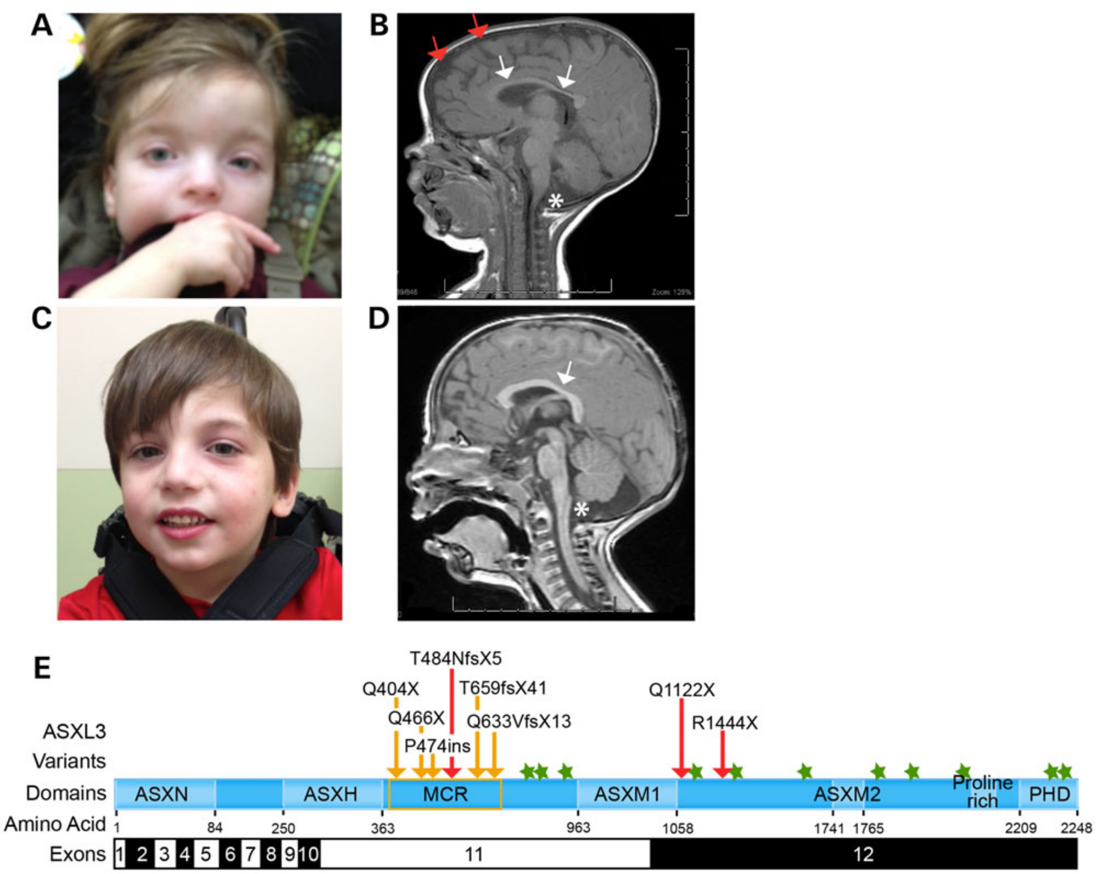

Figure 1. Characterization of pathogenic truncating *ASXL3* variants. (**A**) Facial characteristic of proband I at age 36 months showing low-set ears, broad nasal bridge, sparse arched eyebrows, downslanting palpebral fissures and broad forehead with periorbital fullness. (**B**) Brain MRI of proband I showing cerebellar vermal hypoplasia (single star), corpus callosum hypoplasia (white arrows), increased subdural space (two red arrows) and decreased white matter volume. (**C**) Proband II has a small chin, downslanting palpebral fissures and borderline low-set ears. (**D**) Proband II showing cerebellar vermal hypoplasia (single star) and a shortened corpus callosum (white arrow). (**E**) Schematic illustration of the main functional units of ASXL3 and pathogenic variants. Novel *ASXL3* variants are depicted by red arrows. Previously described truncating *ASXL3* variants (orange arrows cluster in the MCR, orange box). Missense *ASXL3* variants identified in individuals with Autism spectrum disorder (green stars). ASXL3 functional units are shown with corresponding amino acids. *ASXL3* exons 11 and 12 are 1.9 and 3.7 kb in length, respectively, and comprise ~5.6 kb of the ~6.8 kb ASXL3 open reading frame.

in patient fibroblasts, indicating that *ASXL3* nonsense mutations disrupt the normal activity of the PR-DUB complex. Transcriptome analysis of proband and control fibroblasts show significant changes in transcriptional regulation that correlate with altered H2AK119Ub1 levels. While germline mutations in PRC1 complex components were previously shown to disrupt H2A mono-ubiquitination in ASD and primary microcephaly (19,20), BRS is the first single gene disorder exhibiting defects in deubiquitination of H2AK119Ub1. These findings highlight a role for dynamic regulation of H2A ubiquitination in development and disease.

Results

Clinical features of novel *de novo* truncating *ASXL3* variants

Clinical exome sequencing (CES) is often performed on probands with a potential genetic disease, but without a clear diagnosis. We describe three cases for which novel *de novo* heterozygous truncating mutations in *ASXL3* were identified by CES. A summary of clinical findings is presented in Table 1. Proband I is a female born by cesarean section at 38 weeks of gestation following a pregnancy complicated by intrauterine growth retardation that was first evident at 18 weeks of gestation. Her birth weight was 2.25 kg (5% for gestational age), and she was 44.4 cm long (<3% for gestational age). Proband I experienced failure to thrive, feeding problems that included a poor suck reflex and delayed gastric emptying that required a G-tube by 8 months of age. When examined at 5 years 6 months of age, her height and weight were 108 cm (24th percentile) and 15.8 kg (4th percentile).

Proband I presented with dysmorphic facial features that included square facies, downslanting palpebral fissures, low-set ears, broad nasal bridge, small short nose and micrognathia (Fig. 1A). Proband I experienced hyperopia and left-sided esotropia that was successfully repaired. Hypotonia was noted at the neonatal neurological examination. She has global developmental delay and at 6 years of age was unable to sit, crawl or stand independently. Proband I does not communicate verbally and presents with ID. A brain MRI performed at 7 months of age showed a reduction in white matter and cerebral volume together with an increased subdural space most predominantly surrounding the frontal lobes (Fig. 1B). Structurally, thinning of the corpus callosum and hypoplasia of the inferior cerebellar vermis were also observed. Unlike other cases of BRS, Proband I experienced staring

Table 1. Phenotypic features associated with truncating *ASXL3* variants

ASXL3 variant	c.4330T>C	c.3664C>T	c.1448dupT	c.1210C>T	c.1396C>T	c.1975_1978 delACAG	c.1421insT	c.1897_1898 delCA
a.a. Position	p.R1444X	p.Q1122X	p.484NfsX5	p.Q404X	p.Q466X	p.T659fsX41	p.P474fs	p.Q633VfsX13
Identification	Novel University of Michigan			Bainbridge *et al.*				Dinwiddie *et al.*
Craniofacial features								
Trigonocephaly	−	−	+	−	−	−	−	+
Microcephaly	−	−	−	+	+	−	−	+
Prominent forehead	−	−	+	−	−	+	+	NA
Arched eyebrows	−	+	+	+	+	−	+	NA
Prominent eyes	−	−	−	−	−	−	−	+
Astigmatism	−	−	Hyperopia	NA	NA	NA	NA	Myopia
Palpebral fissures	Downslanting	−	Downslanting	−	−	−	−	Upslanting
Nasal bridge	−	−	Broad	−	−	−	−	Depressed
Short/small nose	+	−	+	−	+	+	−	NA
Anteverted nares	+	−	−	+	+	+	+	+
Posteriorly rotated ears	−	−	−	+	+	−	−	+
Low-set ears	−	−	+	−	−	−	+	NA
Small chin	+	−	+	NA	NA	NA	NA	NA
Neurological features								
Brain MRI	WM[a]	NA	WM[a]	NA	NA	NA	WM[b]	WM[c]
Seizures	−	−	+	−	−	−	−	+
ID	+	NA	+	−	−	+	−	+
Absence of speech	+	+	+	+	+	+	+	+
Hypotonia	+	+	+ (axial)	−	+	+	−	+ (axial)
Developmental delay	+	+	+	+	+	+	+	+
Other features								
Gastric tube	+	+	+	+	+	−	+	+
IUGR	+	−	+	+	+	−	+	+
Failure to thrive	+	+	+	+	+	+	+	+
Feeding difficulties	+	+	+	+	+	+	+	+
Precocious puberty	NA	−	+	NA	NA	NA	NA	NA
Recurrent infections	+	−	−	NA	NA	NA	NA	+
Ulnar deviation	−	+	−	+	+	−	+	−

NA, not accessed; MRI, magnetic resonance imaging; ID, intellectual disability; IUGR, intrauterine growth restriction; +, present; −, absent/normal.

[a]Global mild white matter volume loss.

[b]Global mild white matter volume loss with normal myelination: secondary brainstem hypoplasia; Hypoplasia/dysplasia of bilateral cerebellar tonsils.

[c]Mild white matter loss with enlarged lateral ventricles and mild prominence of the sulci.

spells starting at 8 months that resolved by Age 2 and were not accompanied by any electroencephalogram (EEG) changes. Her blood lactate, plasma amino acids and urine organic acids were normal.

Proband II is a male born at 39 weeks by vaginal delivery following a pregnancy complicated by reduced fetal movement. At birth, he weighed 3.4 kg (25th percentile) and was 50.8 cm long (50th percentile). Reduced tone was noted immediately following vaginal delivery. Proband II has a history of failure to thrive and feeding difficulties. Prominent gastrointestinal symptoms included reflux, chronic constipation and oral aversion that required G-tube feedings. Metabolically, his blood lactate, plasma amino acids and urine organic acids were also normal. Proband II presented with minor dysmorphic features, which included a small nose with anteverted nares, a small chin and downslanting palpebral fissures (Fig. 1C).

Neurological exams throughout noted hypotonia and severe delays in meeting developmental milestones. Proband II began pulling to standing at 16 months, but lacks sufficient coordination to walk independently at 4 years of age. He has ID and often acts aggressively. He can mimic a few words but does not use them for communication. The cerebral cortex was structurally normal by MRI, while vermal hypoplasia of the cerebellum and a shortened corpus callosum were noted (Fig. 1D). Proband II experienced recurrent ear infections and had a tonsillectomy. He also experiences joint swelling accompanied by episodes of hand and foot discoloration that are attributed to acrocyanosis.

Proband III is a male who was born at 40 weeks via cesarean section. His birth weight was 3.1 kg (50th percentile) and length 49.53 cm (25th percentile). Proband III has feeding difficulties that have not resolved by 13 months. He was found to have ankyloglossia and had a frenulotomy. Initial concerns about his development started at 7 months of age when he failed to meet gross-motor milestones. At 13 months, he was unable to roll over and sit upright. His neurological exam was remarkable for hypotonia. No dysmorphic features were observed.

All three probands received a detailed clinical evaluation and had a normal oligonucleotide chromosomal microarray before CES was ordered at GeneDx or Ambry Genetics. Trio-CES (proband, mother and father) was performed at GeneDx for Proband I and identified a *de novo* ASXL3 (NM_030632) c.1448dupT frameshift insertion that creates a premature stop codon 5 amino acids (p.T484NfsX5) downstream of the insertion, in exon 11 of *ASXL3* (Fig. 1E). This truncating variant creates a premature stop in the same region of *ASXL3* as the five previously described *de novo* truncating and nonsense *ASXL3* variants, supporting a genetic diagnosis of BRS for this proband (2,4).

CES of Proband II and his mother identified a heterozygous *ASXL3* c.4330T>C, p.R1444X nonsense mutation in Proband II that was not present in his mother (Fig. 1E). The father was not available for testing. Trio-CES, performed at Ambry Genetics for Proband III, discovered a *de novo* heterozygous *ASXL3* c.3364C>T, p.Q1122X nonsense variant (Fig. 1E). Both of these *ASXL3* variants fall outside the original cluster of mutations previously described in exon 11 and instead localize to the 5′ end of exon 12, expanding the clinical significance of nonsense variants throughout *ASXL3* in BRS. Mosaicism was not investigated to determine the timing of these *de novo* events.

Truncating *ASXL3* variants result in loss-of-function alleles

The N-terminal ASXN and ASXH domains of ASXL3 are predicted to act as a scaffold to mediate interactions with protein complexes (11,12,17,21,22). In contrast, the C-terminal ASXM2 domain and PHD finger recognize chromatin histone post-translational modifications (PTMs) (12,23,24). The first pathogenic variants identified in *ASXL3* clustered between these two C- and N-terminal functional components, raising the possibility that stably expressed truncated proteins may uncouple the ASXL3 scaffolding interactions and chromatin reader activities, allowing the truncated protein to act as a dominant negative (2). To investigate this scenario, a primary dermal fibroblast line was established from Proband I, who is heterozygous for a frameshift variant within the mutational cluster region of *ASXL3* ($ASXL3^{+/fs}$ fibroblasts; Fig. 1E). A C-terminally V5/His tagged full-length ASXL3 (fl-ASXL3-V5/His) and truncated ASXL3 (tr-ASXL3-V5/His) fragment potentially expressed from the *ASXL3* c.1448dupT allele were also generated (Fig. 2A). A total of 293 T overexpressed tr-ASXL3-V5/His was analyzed concurrently with whole cell lysate from $ASXL3^{+/+}$ and $ASXL3^{+/fs}$ fibroblasts. The α-ASXL3 antibody recognizes tr-ASXL3-V5/His. However, a similarly sized band was not detected in either $ASXL3^{+/+}$ or $ASXL3^{+/fs}$ fibroblasts, indicating the *ASXL3* c.1448dupT variant does not express a stable protein (Fig. 2D). To evaluate the impact of this frameshift mutation on expression of full-length ASXL3, the 280 KDa band, corresponding to the fl-ASXL3-V5/His band, was quantified from $ASXL3^{+/+}$ and $ASXL3^{+/fs}$ fibroblast whole cell lysates (Fig. 2B). Expression of endogenous ASXL3 in $ASXL3^{+/fs}$ fibroblasts was 50% of that quantified in control fibroblasts after normalization to β-actin (Fig. 2C), reflecting the sensitivity of BRS pathology to reduced dosage of *ASXL3*.

De novo truncating *ASXL3* variants are predicted to promote nonsense-mediated decay (NMD). To investigate the dynamics of mRNA stability, mutant *ASXL3* mRNA transcripts were quantified from control and $ASXL3^{+/fs}$ fibroblast cDNA. Quantitative real-time polymerase chain reaction (qRT–PCR) of *ASXL3* and *GAPDH* were performed in triplicate. Normalized *ASXL3* transcripts from patient cDNA were 61% of the transcripts detected in controls (Fig. 2E), suggesting the c.1448dupT transcripts undergo NMD. To directly quantify the ratio of *ASXL3* reference to c.1448dupT transcripts, an amplicon spanning the pathogenic variant was sequenced. The *ASXL3* c.1448dupT genotype was detected in 12.8% of a total 112 000 reads covering the amplicon generated from $ASXL3^{+/fs}$ fibroblast cDNA. The *ASXL3* c.1448dupT transcript was not detected in 127 000 reads covering the amplicon generated from $ASXL3^{+/+}$ fibroblast cDNA. These results suggest that the *ASXL3* c.1448dupT transcript is sensitive to NMD and contributes to the reduced *ASXL3* transcript level and protein expression in Proband I fibroblasts (Fig. 2D).

Truncating *ASXL3* mutations alter H2A ubiquitination

ASXL1 and ASXL2 possess a conserved N-terminal BAP1-binding site, with ASXL3 exhibiting 89% homology across these same amino acids (11). The BAP1-binding site is 5′ of the ASXL3 p.T484NfsX5 variant and covered by the tr-ASXL3-V5/His ASXL3 fragment. To determine whether ASXL3 also interacts with BAP1, flag-tagged BAP1 (BAP1-Flag) and tr-ASXL3-V5/His were overexpressed and co-immunoprepitpated (co-IP) from 293 T cells (Fig. 3A). When co-overexpressed with BAP1-Flag, a fraction of tr-ASXL3-V5/His is post-translationally modified, generating a larger band by western blot not observed when tr-ASXL3-V5/His is overexpressed alone. The PTM shifts the tr-ASXL3-V5/His band size in excess of what would be predicted for phosphorylation alone and was confirmed following incubation of co-overexpressed cell lysates with calf intestinal phosphatase (CIP) (Supplementary Material, Fig. S1). Reciprocal co-IP was performed with both

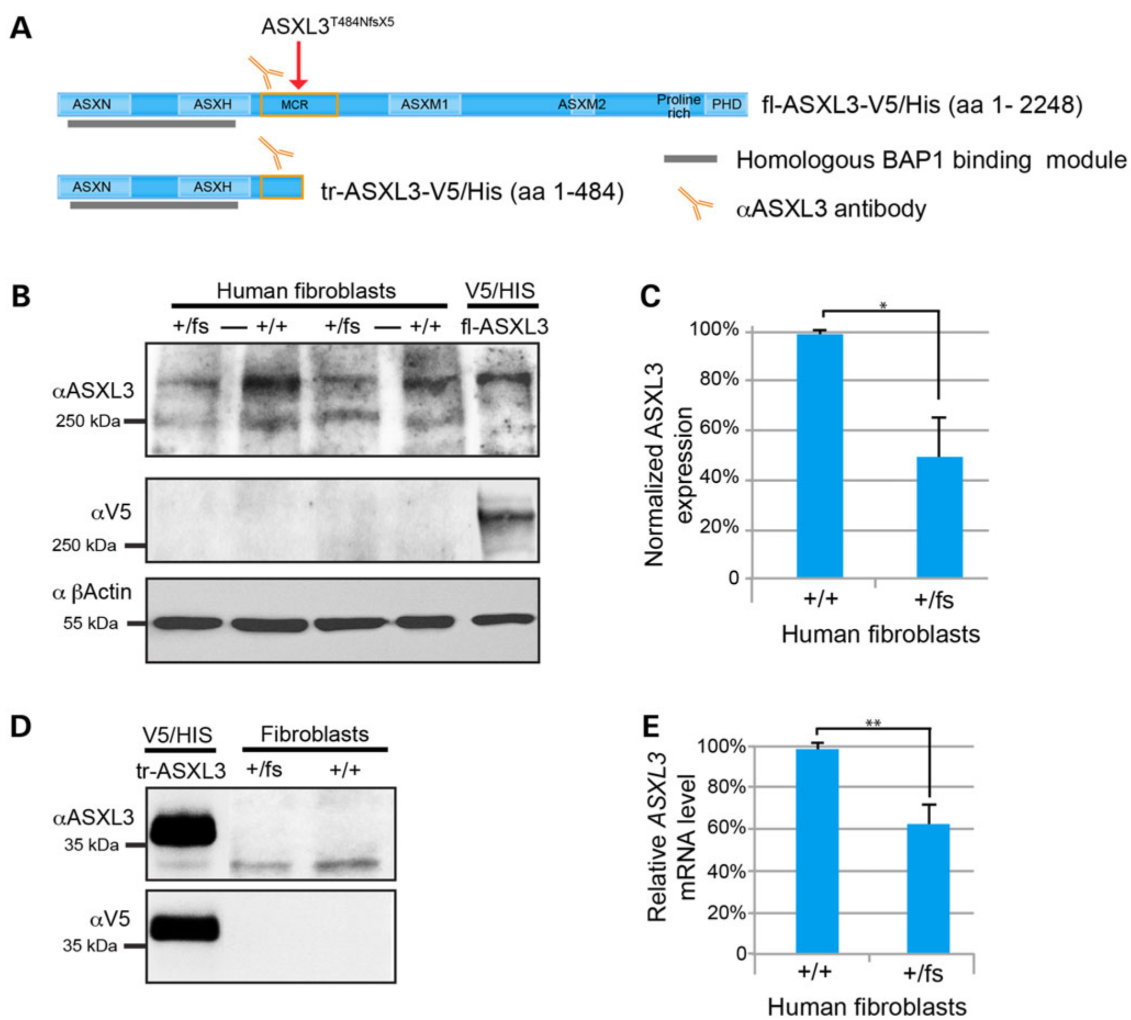

Figure 2. Characterization of truncating ASXL3 variants in patient fibroblasts. (**A**) Schematic of ASXL3 C-terminally V5/His tagged constructs and length in amino acids (aa), the region of ASXL3 recognized by the α-ASXL3 antibody (orange antibody), ASXL3 N-terminus that shares 89% homology with the BAP1-binding region of ASXL1 and 2 (gray bar), proband I truncating variant (red arrow). (**B**) Western blot of two biological replicates comparing endogenous full-length ASXL3 expression in patient $ASXL3^{+/fs}$ and control $ASXL3^{+/+}$ fibroblasts (+/fs to +/+). Overexpressed fl-ASXL3-V5/His runs at ∼280 kDa, corresponding to the highest molecular weight band from fibroblast cell lysates recognized by the α-ASXL3 antibody. fl-ASXL3-V5/His is recognized by α-ASXL3 and α-V5 antibodies. β-Actin was used as a loading control. (**C**) Quantification of endogenous full-length ASXL3 protein in $ASXL3^{+/fs}$ and control $ASXL3^{+/+}$ fibroblasts relative to expression of β-actin, $n = 3$ (Error bars denote SD; $^{*}P = 0.04$). (**D**) Overexpressed tr-ASXL3-V5/His is recognized by α-ASXL3 and α-V5 antibodies. A band of comparable molecular weight is not detected in $ASXL3^{+/fs}$ and control $ASXL3^{+/+}$ cell lysate. (**E**) qRT–PCR analysis of ASXL3 transcripts from $ASXL3^{+/fs}$ and control $ASXL3^{+/+}$ fibroblasts cDNA relative to GAPDH, $n = 3$ (Error bars denote SD; $^{**}P = 0.005$).

α-Flag and α-V5 antibodies. As shown in Figure 3A, the two proteins interact when co-immunoprecipitated with either antibody; however, BAP1-Flag preferentially interacts with the post-translationally modified tr-ASXL3-V5/His. This indicates that ASXL3 interacts with BAP1, making up the components of the PR-DUB complex. In addition to phosphorylation, ASXL3 can be poly-ubiquitinated at K350, which may account for the additional tr-ASXL3-V5/His band shifted ∼20 kDa larger when co-expressed with BAP1-flag (PhosphoSite.org). The specific PTM that contributes to this interaction will be investigated in future experiments.

PcG proteins form multi-subunit, chromatin-modifying complexes that maintain transcriptional repression in multicellular organisms. While the molecular functions of Polycomb repressive complexes 1 and 2 (PRC1 and PRC2) have been subject to intense scrutiny, the role of PR-DUB is less well described (16). PRC2 is well known for its role in histone H3 trimethlyation of lysine 27 (H3K27me3). PRC1 is responsible for the majority of H2AK119Ub1 across the genome, while PR-DUB removes this histone PTM (16). Loss of Ring1b, an E3 ubiquitin ligase associated with PRC1, leads to reduced H2AK119Ub1, release of the paused polymerase and gene de-repression (25–27). To investigate the impact of *ASXL3* mutations on the global level of H2A mono-ubiquitination, we measured the H2AK119Ub1 level of acid extracted histones from control and $ASXL3^{+/fs}$ fibroblasts. Genome-wide H2AK119Ub1 level in $ASXL3^{+/fs}$ fibroblasts was elevated 5-fold above control cells when normalized to histone H3 (Fig. 3B). *ASXL1* loss-of-function mutations have been shown to also alter the levels of H3K27me3 (28,29); however, the level of H3K27me3 was unchanged in $ASXL3^{+/fs}$ fibroblasts. These studies suggest the ASXL3-specific PR-DUB complex may confer distinct molecular functions independent of other ASXL family members.

Transcriptome altered in $ASXL3^{+/fs}$ skin fibroblasts

To analyze the impact of elevated H2AK119Ub1 on transcriptional regulation in $ASXL3^{+/fs}$ fibroblasts, we conducted a genome-wide analysis of mRNA levels for three biological replicates of $ASXL3^{+/fs}$ and $ASXL3^{+/+}$ fibroblast lines. Highly reproducible

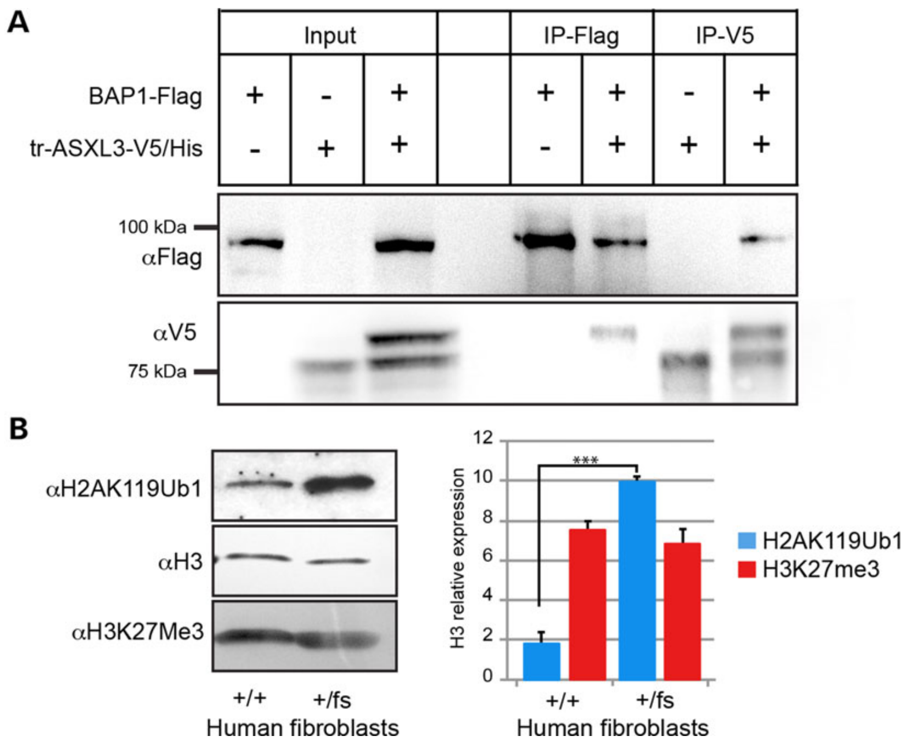

Figure 3. ASXL3 interacts with BAP1 and truncating mutations alter histone H2A ubiquitination. (**A**) BAP1-Flag and tr-ASXL3-V5/His were individually and co-overexpressed in 293 T. The N-terminal fragment of ASXL3 is post-transcriptionally modified when co-overexpressed together with BAP1-Flag and is seen as a doublet in the corresponding lane. Reciprocal co-immunoprecipitations were performed with α-V5 and α-flag antibodies. BAP1-Flag preferentially binds the post-transcriptionally modified tr-ASXL3-V5/His fragment. (**B**) H2AK119Ub1 and H3K27Me3 acid extracted histones levels compared between *ASXL3*$^{+/+}$ and *ASXL3*$^{+/fs}$ fibroblasts. H3 used as loading control. A 5-fold increase in H2AK119Ub1 was quantified in *ASXL3*$^{+/fs}$ fibroblasts compared with H3 levels. No change detected in normalized H3K27Me3 acid extracted histone levels between *ASXL3*$^{+/+}$ and *ASXL3*$^{+/fs}$ fibroblasts, $n = 3$ (Error bars denote SD; ***P = 0.001).

changes in the transcriptome were observed in *ASXL3*$^{+/fs}$ cells with 564 genes showing significant changes in transcription (false discovery rate adjusted *P*-values defined by DEseq2, $q < 0.05$ and $\log_2$ fold change in expression of ≥1). Despite the genome-wide increase in H2AK119Ub1 and its potential to repress transcription overall, the transcriptional levels observed in fibroblasts from both genotypes were highly correlated (Pearson correlation coefficient r^2—0.96), indicating that global transcriptional activity is not altered in *ASXL3*$^{+/fs}$ fibroblasts. Of the 564 differentially expressed genes (DEGs) in *ASXL3*$^{+/fs}$ fibroblasts, 48% (254) were significantly downregulated and 52% (310) significantly up-regulated (Fig. 4A). Five percent of the transcripts were non-coding RNA that were distributed between up- and downregulated transcripts. Fifteen of the significant DEGs were confirmed by qRT–PCR from both proband and control fibroblasts and normalized to *GAPDH* (Supplementary Material, Fig. S2). The comparable number of up- and downregulated genes suggests that the function of ASXL3 is required to both silence and activate genes in a cellular-dependent context, a function of this gene family that has been conserved across evolution (8–10,30).

In *ASXL3*$^{+/fs}$ fibroblasts, *HOX* transcripts were highly repressed. Differentially expressed HOX transcripts were specific to contiguous *HOX* genes, the *HOXA* and *HOXC* clusters, and included the intervening long non-coding RNA (lncRNA) at both loci. On Chromosome 7, *HOXA7*, *HOXA10*, *HOXA11* and *HOXA13* are repressed, as well as the HOXA10-AS and HOXA11-AS lncRNA that reside in the intervening sequence at that chromosomal locus. A similar configuration is observed on chromosome 12 where *HOXC10*, *HOXC11*, *HOTAIR*, *HOXC-AS1*, *HOXC-AS2* and *HOXC-AS3* are all significantly repressed. The top up-regulated genes depicted on the volcano plot were components of the extracellular matrix (Fig. 4B).

To better understand the functional impact of transcriptional changes occurring, we performed enrichment analysis of Gene Ontology (GO) categories on pooled proband I and control fibroblast transcriptomes (31–33). DEGs from our dataset were enriched in GO terms that underscore the role of *ASXL3* in transcriptional regulation, development and proliferation, i.e. positive regulation of transcription from RNA polymerase II promoter, endoderm differentiation, proximal/distal limb development, early digestive track development, negative regulation of astrocyte differentiation, growth factor activity and negative regulation of cell proliferation. The top GO terms from this analysis are specified in Table 2. These findings are consistent with the features of failure to thrive, global developmental delay, reduced brain volume, ID, dysmorphic features and feeding problems observed in BRS. It will be important to determine whether DEGs enriched in the GO terms 'extracellular matrix organization' and 'integral components of plasma membrane' contribute to the clinical features of BRS.

The molecular pathways impacted by DEGs in BRS are poorly understood. To explore the disrupted molecular pathways that can be inferred from our data, we performed impact analysis with iPathway tools to identify interactions among DEGs that predict significantly affected Kyoto Encyclopedia of Genes and Genomes (KEGG) pathways (34–39). This analysis quantifies two independent probabilities: (i) over-representation of DEGs in a given pathway (*P*-Acc) and (ii) perturbation of a pathway computed by propagating the measured expression changes across the pathway topology (*P*-ORA). Five KEGG pathways were found

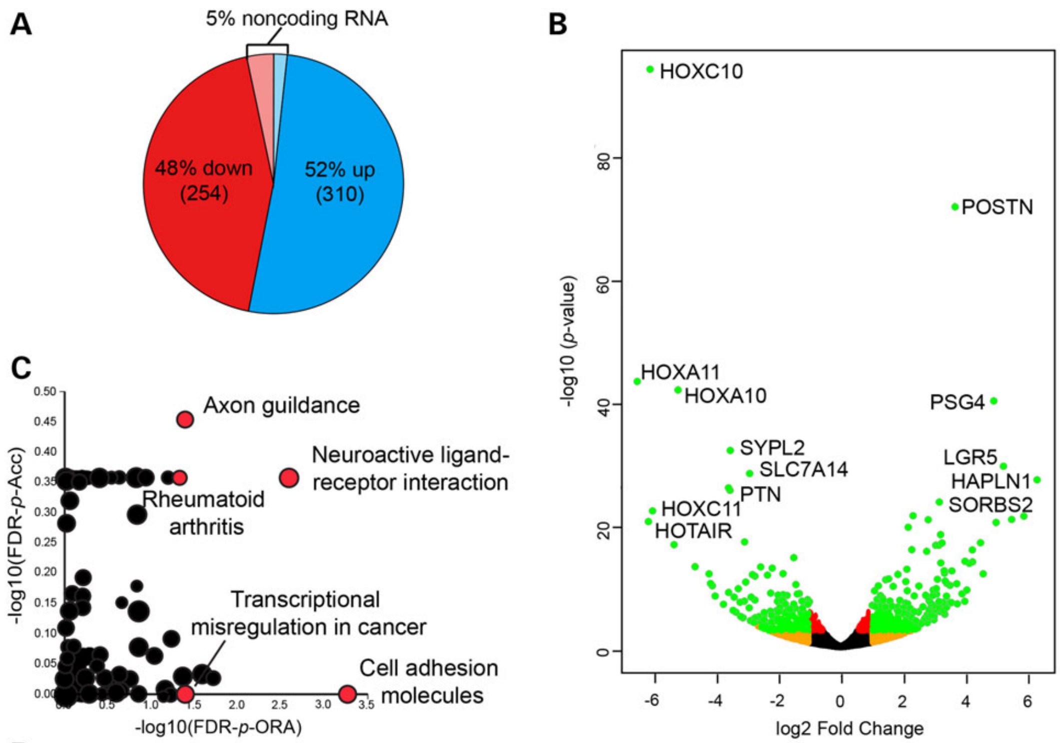

D

KEGG Pathway	Name	FDR-p-value
KEGG: 04514	Cell adhesion molecules (CAM)	5.44e-4
KEGG: 04080	Neuroactive ligand-receptor interaction	0.004
KEGG: 04360	Axon guidance	0.004
KEGG: 05323	Rheumatoid arthritis	0.023
KEGG: 05202	Transcriptional misregulation in cancer	0.048

Figure 4. Transcriptome analysis of *ASXL3*$^{+/fs}$fibroblasts. (**A**) Percentage of differentially up- and down- regulated transcripts in *ASXL3*$^{+/fs}$ fibroblasts. Five percent of differentially expressed transcripts were identified as non-coding RNA. (**B**) Volcano plot: all 564 significant DEGs (green dots) are represented in terms of their measured expression change ($\log_2$ fold change) and the significance of their change [$-\log_{10}$ (P-value)]. The significance is represented in terms of the negative log of the *P*-value. (**C**) Red circles are KEGG pathway with significant normalized enrichment scores according to the false discovery rate *P*-value (FDR *P*-value) corrected for multiple hypothesis testing. The impact of each pathway is plotted relative to the number of DEGs enriched in each pathway (*p*-Acc) and the perturbation (*p*-ORA) of the pathway based on the measured expression changes across the pathway topology. Black dots represent KEGG pathways that do not reach significance according to FDR *P*-value calculated. (**D**) Significantly enriched KEGG pathways and their FDR *P*-value.

to be significantly impacted: (i) Cell adhesion molecules, (ii) Neuroactive ligand-receptor interaction, (iii) Axon guidance, (iv) Rheumatoid arthritis and (v) Transcription misregulation in cancer (Fig. 4D). DEGs were both enriched and highly dysregulated in the 'Rheumatoid arthritis', 'Axon guidance' and 'Neuroactive ligand-receptor interaction' pathways, compared with the 'Transcriptional misregulation in cancer', and 'Cell adhesion molecules' pathways were specified by the enrichment of DEGs alone. The DEGs in each KEGG pathway are outlined in Supplementary Material, Figure S3. Understanding the gene expression signatures and their impact on molecular pathways will provide a better understanding of key gene targets responsible for features of BRS.

Discussion

Here we describe three novel variants in *ASXL3* that contribute to our understanding of the clinical spectrum and molecular impact of truncating mutations in BRS. The three probands we describe fit within the phenotypic spectrum previously described for BRS. These data suggest that the phenotypic variability is not directly correlated with the placement of the truncating mutations in *ASXL3*, as two of the variants we describe do not fall within the original cluster of mutations. The distinct phenotypic features observed in individual BRS probands are outlined in Table 1; however, the most pervasive characteristics are non-specific features. Most prominent among them are feeding difficulties that are present from birth and often require intervention. Psychomotor delays are observed, starting with the earliest milestones. Several probands were small at birth and failed to thrive. Likewise, the degree of ID is variable; however, all are non-verbal or experience significant communication difficulties.

The genetic variation originally published for *ASXL3* suggested that pathogenic truncating variants in *ASLX3* might function in a dominant-negative manner. First, the original mutations clustered in the penultimate exon of *ASXL3* (2,4), bisecting the N-terminal protein scaffolding functions of the gene from the C-terminal chromatin/DNA-targeting activities (12). Second, nonsense mutations both 5′ and 3′ of the mutational cluster region (MCR) are observed in databases composed of sequence

Table 2. Gene ontology categories enriched with BRS fibroblast DEGs

GO accession	Name	P-value (elim pruning[a])
Biological process		
GO:0030198	extracellular matrix organization	2.400e−7
GO:0045944	positive regulation of transcription from RNA polymerase II promoter	2.00e−5
GO:0009954	proximal/distal pattern formation	3.500e−5
GO:0048566	embryonic digestive tract development	6.300e−5
GO:0008285	negative regulation of cell proliferation	7.600e−5
GO:0070836	caveola assembly	7.900e−5
GO:0001706	endoderm formation	1.000e−4
GO:0048712	negative regulation of astrocyte differentiation	1.100e−4
Cellular component		
GO:0005887	integral component of plasma membrane	6.000e−13
GO:0005615	extracellular space	2.100e−9
GO:0005578	proteinaceous extracellular matrix	1.600e−8
GO:0001725	stress fiber	7.700e−6
Molecular function		
GO:0008083	growth factor activity	1.300e−6
GO:0008201	heparin binding	2.800e−5
GO:0043565	sequence-specific DNA binding	4.400e−5
GO:0001077	transcriptional activator activity, RNA polymerase II core promoter proximal region sequence-specific binding	1.900e−4
GO:0008330	protein tyrosine/threonine phosphatase activity	2.800e−4
GO:0042803	protein homodimerization activity	4.800e−4

[a]For each Gene Ontology (GO) term (31,32), the number of DEG annotated to the term is compared with the number of genes expected just by chance. Given the nature of the gene ontology, this introduces errors by considering genes multiple times. To overcome this limitation, the elim method was used to iteratively remove genes that map to significantly enriched GO term (33).

variants from phenotypically normal individuals (2). Our data show that the *ASXL3* c.1448dupT variant is subject to NMD (Fig 2D) and not expressed in *ASXL3*$^{+/fs}$ fibroblasts consistent with loss-of-function mutations (Fig 2B). While these data argue against a dominant-negative genetic mechanism, these findings do not address the *ASXL3* nonsense mutations that populate sequence databases composed of phenotypically normal individuals. In these cases, *ASXL3* nonsense mutations may represent mutations arising post-zygotically or during later embryogenesis and thus may be explained by the timing of these *de novo* mutational events and mosaicism (40,41). This explanation is supported by the high incidence of somatic mutations in *ASXL* genes observed in various types of cancers (14,42–52). The timing of *de novo* mutational events during development may also account for some of the phenotypic variability exhibited between BRS patients with similar *ASXL3* nonsense variants.

While ASXL3 and ASXL1 share homology that allows both proteins to interact with similar binding partners, the divergent genetics and molecular pathology corresponding to their respective germline and somatic mutations suggest distinct molecular mechanisms. In *ASXL3* genetics, somatic mutations are observed primarily in melanoma, and only *ASXL3* missense have has been observed in individuals with ASD. These genetic findings also link *ASXL3* to other encoded chromatin remodelers, namely *KDM5B*, *KMT2C*, *KMT2H* and *NSD2* (3). Molecularly, our data revealed elevated H2AK119Ub1 in *ASXL3*$^{+/fs}$ primary fibroblasts, while changes in the H3K27Me3 were unchanged (Fig 3B). In contrast, *ASXL1, ASXL2, DNMT3A, EZH2, IDH1, IDH2, KMT2A* and *TET2* genes are altered in myelodysplastic syndrome and acute myeloid leukemia (14,42,43,53–56), while *ASXL3* mutations are conspicuously lacking (57). Likewise, changes in H3K27Me3 are the molecular signature attributed to germline and somatic mutations in *ASXL1*. Consequently, despite some overlapping clinical features, BRS may be molecularly distinct from Bohring-Opitz syndrome (OMIM 605039) caused by *de novo* mutations in *ASXL1*.

Few genes that impact the dynamic regulation of H2A mono-ubiquitination have been identified in human genetic studies. Human variants have been observed in *autism susceptibility candidate 2* (*AUTS2*) and *Polyhomeotic-like 1* (*PHC1*), which encode non-canonical and canonical PRC1 components, respectively, and disrupt mono-ubiquitination of H2A (19). Copy number variants of *AUTS2* have been observed in individuals with ID (OMIM 615834) (58,59), while homozygous missense mutations in *PHC1* were identified in a consanguineous family with primary microcephaly (OMIM 615414) (20). Likewise, reduced H2AK119ub1 levels have also been described in Down syndrome (OMIM 190685) due to increased dosage of *Ubiquitin-specific protease 16* (*USP16*), which encodes ubiquitin carboxyl-terminal hydrolase 16. Reduced H2AK119ub1 was correlated to decreased proliferation of normal fibroblasts and postnatal neural progenitors and accelerated senescence (60). Conversely, *Usp16* null mouse embryonic stem cells exhibit delayed lineage commitment and persistent self-renewing proliferation (61). These findings accentuate the sensitivity of growth and developmental mechanisms to the dosage of genes that impact H2A mono-ubiquitination regulatory mechanisms. Truncating mutations in *ASXL3* are the first to link the pathology of a single gene disorder to elevated levels of H2AK119Ub1. This finding also illuminates an important role for dynamic regulation of H2A mono-ubiquitination in development, that when disrupted can result in features of Autism and ID.

Consistent with the growth deficits observed in BRS, many DEGs identified from transcriptome analysis of *ASXL3*$^{+/fs}$ and *ASXL3*$^{+/+}$ fibroblasts were enriched in GO terms defined by proliferation and growth. Cdkn2a is a well-characterized PRC1 target locus in fibroblasts, which encodes p16^{Ink4a} and p19^{Arf}, tumor suppressors involved in senescence-induced loss of proliferation (62–65). The Cdkn2a locus is also sensitive to changes in

H2AK119KUb1 (60,66); however, it is not differentially expressed in *ASXL3*$^{+/fs}$ fibroblasts. Instead, *ASXL3*$^{+/fs}$ DEGs were enriched in the GO terms 'negative regulation of cell proliferation' (GO:0008285; Table 2) and 'growth factor activity' (GO:0008083), which may represent alternative mechanisms that contribute to the reduced growth phenotypes in BRS. Likewise, seven DEGs were significantly enriched in the GO term for embryonic digestive tract development (GO:0048566; *PCSK5, RARRES2, ALDH1A2, PKDCC, FOXF2, ADA* and *GLI2*), which is pertinent given the feeding difficulties observed in BRS patients.

A number of repressed *HOX* genes were enriched in the proximal/distal pattern formation GO term (GO:0009954), and differential regulation of *HOX* genes may contribute to the ulnar deviation phenotype that is observed in 4 of the 8 described BRS patients. However, the role of ASXL3 in transcriptional regulation of *HOX* genes during development has yet to be determined. Human genetics has revealed the clinical manifestations of germline pathogenic variants in *HOXA11* and *HOXA13*, but few phenotypic features overlap with BRS. Dominant truncating variants in *HOXA11* lead to radioulnar synostosis with amegakaryocytic thrombocytopenia (OMIM 605432), while dominant truncating and missense variants in *HOXA13* are associated with hand-foot-genital syndrome (OMIM 140000) or Guttmacher syndrome (OMIM 176305), respectively (67). These disorders highlight the digit and urogenital malformations that are often associated with *HOXA* mutations and suggest that heterozygous truncating variants in *ASXL3* may not be critical for spatial and temporal developmental repression of *HOXA* genes required to generate these phenotypes.

KEGG analysis highlights the combinations of DEGs that may contribute to BRS pathology. Our pathway analysis identified several KEGG pathways consistent with BRS features. Additional experimental work will need to be performed to determine whether DEGs enriched in the 'Axon guidance' pathway contribute to the thin corpus callosum, observed in Proband I. This approach could provide insights concerning the best treatment options to pursue (Supplementary Material, Fig. S3). Given the role of ASXL family members in cancer, enrichment of DEGs in the 'Transcriptional misregulation in cancer' pathway is well supported by the published literature. The added cancer risk conferred by germline mutations in *ASXL3* has not been determined and will need to be assessed for children and adults carrying mutations in this gene.

In conclusion, BRS patient primary fibroblasts were used to investigate the molecular defects associated with truncating variants in *ASXL3*. Our data highlight an important role for ASXL3 in specifying H2AK119Ub1 levels, a molecular feature sensitive to the dosage of genes that impact H2A mono-ubiquitination. These findings will aid in the future development of appropriate models to investigate the role of this chromatin modification in BRS.

Materials and Methods

Establishment primary skin fibroblast line

Punch skin biopsies were taken from the upper back for proband I and controls at the University of Michigan. All procedures followed were in accordance with the ethical standards of the University of Michigan Medical School IRB, and an informed consent was obtained. A primary skin fibroblast line was established according to a previous published protocol (68).

Western blot analyses and antibodies

Primary fibroblast cells were lysed with 50 mm Tris–HCl pH 7.4, 1% NP-40, 0.25% Na-deoxycholate, 150 mm NaCl, 1 mm EDTA, 1 mm Na-vanadate and 1 mm phenylmethylsulfonyl fluoride (PMSF), supplemented with protease inhibitor cocktail and phosphatase inhibitor cocktail 3 obtained from Sigma-Aldrich (P8340 and P0044; St Louis, MO, USA) and were normalized for protein content using Bradford assay and β-actin. Cell lysates were separated using electrophoresis on 6 and 10% SDS-polyacrylamide gels and transferred to PVDF membrane (Millipore, Billerica, MA, USA). For western blot, after the transfer, the PVDF membrane was blocked with 4% milk and incubated with following antibodies overnight. Primary antibodies used were: α-ASXL3 (NAP2-14791; Novus Biologicals, Littleton, CO, USA), α-ubiquityl-Histone H2A, α-V5 (05-678 and 46-0705; Millipore, Billerica, MA, USA), α-Histone H3 tri methyl K27, α-Histone H3 antibody (ab6002, and ab1791; Abcam Cambridge, MA, USA), α-FLAG (F3165; Sigma-Aldrich). HRP-conjugated secondary antibodies sc-2005, sc-2030 from Santa Cruz Biotechnology (Dallas, TX, USA) were used for 1 h incubation at room temperature. Antibody incubation and chemiluminescence detection were performed according to manufacturer's instruction [ThermoFisher Scientific (Waltham, MA, USA) cat no. 34095].

Co-immunoprecipitation

In total, 293 T cells were transiently co-transfected with plasmids expressing FLAG-BAP1 and tr-ASXL3-V5/His (aa1-aa484) gene constructs using lipofectamine 3000 (ThermoFisher Scientific, Waltham, MA, USA). Two days following transfection, total cell lysates were prepared with modified RIPA buffer. α-V5 and α-Flag antibodies were incubated with the protein G-coupled (protein G dynabeads, Life Technologies, 1004D) to form a beads-Ab complex. Target antigen was precipitated from the total cell lysate using dynabead-Ab complex. Bound beads were washed 3 times with PBS. Substrate was eluted by boiling in 50 mM glycine buffer pH 2.8 and analyzed by western blot.

Acid extraction of histones from primary fibroblast cell lines

Confluent cells (80–100%) were harvested with TEB [0.5% Triton X 100 (v/v), 2 mм PMSF, 0.02% (w/v) NaN_3], supplemented with 5 mм sodium butyrate at a density of 10^7 cells per ml and lysed on ice for 10 min. Nuclei were pelleted, resuspended in 1/4th volume of 0.2 м HCl overnight. Insoluble material was pelleted, and supernatant containing histones was incubated with sample loading buffer for 10 min. Protein concentration were quantified using Bradford assay.

Generation of fl-ASXL3-V5/His and tr-ASXL3-V5/His constructs

Total RNA was extracted from human neural progenitor cells using RNeasy mini kit (74104, Qiagen, Valencia, CA, USA) according to the manufacturer's instructions. cDNA synthesis on the isolated RNA was then carried out with SuperScript III Reverse Transcriptase using oligo dT primer according to the instructions provided (18080, Invitrogen, Grand Island, NY, USA). Full-length *ASXL3* (fl-ASXL3 forward primer 5′-GCCACCATGAAAGACAA GAGGAAGAAG-3′, fl-ASXL3 reverse primer 5′-TGCTCGTACAA CCAGGCATGCTACAC-3′) and truncated *ASXL3* fragment (tr-ASXL3 forward primer 5′-GCCACCATGAAAGACAAGAGGAA GAAG-3′ and tr-ASXL3 reverse primer 5′-CTGGCATTCACAGA TACTAGTCTCTACCTC-3′) were amplified using Phusion Hot Start II High-Fidelity DNA Polymerase (ThermoFisher Scientific, Waltham, MA, USA). Fragments were gel purified using QIAquick

Gel Extraction kit (28704, Qiagen) and incubated at 72°C with dNTP and Taq polymerase (201205, Qiagen) for 10 min to create 3′ A overhang. Product was ligated into pCDNA3.1-V5-His-Topo (45-0005, Invitrogen).

RNA isolation, library construction and sequencing

Transcriptome libraries were prepared using 200–1000 ng of total RNA. PolyA + RNA isolation, cDNA synthesis, end-repair, A-base addition and ligation of the Illumina indexed adapters were performed according to the TruSeq RNA protocol (Illumina). Libraries were size selected for 250–300 bp cDNA fragments on a 3% Nusieve 3:1 (Lonza) gel, recovered using QIAEX II reagents (QIAGEN) and PCR amplified using Phusion DNA polymerase (New England Biolabs). Total transcriptome libraries were prepared as above, omitting the poly A selection step and captured using Agilent SureSelect Human All Exon V4 reagents and protocols. Library quality was measured on an Agilent 2100 Bioanalyzer for product size and concentration. Paired-end libraries were sequenced with the Illumina HiSeq 2500, (2 × 121 nucleotide read length) with sequence coverage to 50 M paired reads and 100 M total reads.

RNA-sequencing data analysis

Alignment: Paired-end reads were aligned to the human reference genome (GRCh37/hg19) and transcriptome using a RNA-seq spliced read mapper Tophat2 (Tophat 2.0.4) with default settings (69,70). Fragment quantification was computed using feature Counts and annotated according to RefSeq genes. Fragments are only assigned to a gene if it overlaps features of that gene. DESeq2 was used to calculate estimates of dispersion and logarithmic fold changes to perform the expression normalization and differential expression analysis (71). Significantly DEGs were declared to have FDR ≤ 0.1 and $\log_2$ fold change of ≥1. We annotated genes and isoforms with NCBI Entrez GeneIDs and text descriptions. We used ipathway guide (http://www.advaitabio.com/ipathwayguide.html) for enrichment analysis of the set of DEGs to identify significantly enriched functional categories.

Preparation and analysis of miRNA-seq libraries

Total RNA was isolated using RNeasy Kit (Invitrogen) with DNase I digestion according to the manufacturer's instructions from the patient fibroblast cells. cDNA was synthesized from total RNA using Superscript III (Invitrogen) and random primers (Invitrogen). The region harboring the patient mutation c.1448dupT was amplified using the PCR with the product size of 454 bp. Barcode-indexed shotgun sequencing libraries were prepared from *ASXL3* RT-PCR products using Tn5 transposase as previously described (72,73). Shotgun reads were mapped to the human reference assembly build 37 with BWA-MEM (biorxiv, http://arxiv.org/abs/1303.3997) (74). Freebayes (http://arxiv.org/abs/1207.3907) was used to identify variants including the *ASXL3* frameshift and using option '–pooled-continuous' to count the allelic distribution in each sample.

qRT–PCR verification

RNA sequencing findings of several top of DEGs were confirmed by qRT–PCR using the SYBR PCR master mix (Roche Applied Science, Indianapolis, USA). Total RNA was isolated using RNeasy Kit (Invitrogen) with DNase I digestion according to the manufacturer's instructions. RNA integrity was verified on an Agilent Bioanalyzer 2100 (Agilent Technologies, Palo Alto, CA, USA). cDNA was synthesized from total RNA using Superscript III (Invitrogen) and random primers (Invitrogen). Quantitative RT–PCR was performed using Eppendorf Mastercycler® ep realplex according to manufacturer's instructions. Each target was run in triplicate, and expression levels relative to the housekeeping gene *GAPDH* were determined on the basis of the comparative threshold cycle CT method ($2^{-\Delta\Delta}$CT). The primer sequences used in these experiments are given in Supplementary Material, Figure S3C.

Supplementary Material

Supplementary material is available at *HMG* online.

Acknowledgements

We thank Amanda Moccia for assistance with manuscript preparation, Dr Jacob Kitzman and Dr Dan Robertson for technical advice, and genetic counselors Bridget O'Connor and Kailey Owens, who continue to counsel families with BRS patients seen at University of Michigan Pediatrics Medical Genetics.

Conflict of Interest statement. None declared.

Funding

This work was supported by the National Institutes of Health (R00HD069624 to S.L.B., R01 DC009410 to D.M.M.) and by the Donita B. Sullivan Professorship funds to D.M.M.

References

1. Russell, B. and Graham, J.M. (2013) Expanding our knowledge of conditions associated with the ASXL gene family. *Genome Med.*, **5**, 16.
2. Bainbridge, M.N., Hu, H., Muzny, D.M., Musante, L., Lupski, J.R., Graham, B.H., Chen, W., Gripp, K.W., Jenny, K., Wienker, T.F. *et al.* (2013) De novo truncating mutations in ASXL3 are associated with a novel clinical phenotype with similarities to Bohring-Opitz syndrome. *Genome Med.*, **5**, 11.
3. De Rubeis, S., He, X., Goldberg, A.P., Poultney, C.S., Samocha, K., Cicek, A.E., Kou, Y., Liu, L., Fromer, M., Walker, S. *et al.* (2014) Synaptic, transcriptional and chromatin genes disrupted in autism. *Nature*, **515**, 209–215.
4. Dinwiddie, D.L., Soden, S.E., Saunders, C.J., Miller, N.A., Farrow, E.G., Smith, L.D. and Kingsmore, S.F. (2013) De novo frameshift mutation in ASXL3 in a patient with global developmental delay, microcephaly, and craniofacial anomalies. *BMC Med. Genomics*, **6**, 32.
5. Ku, C.S., Polychronakos, C., Tan, E.K., Naidoo, N., Pawitan, Y., Roukos, D.H., Mort, M. and Cooper, D.N. (2013) A new paradigm emerges from the study of de novo mutations in the context of neurodevelopmental disease. *Mol. Psychiatry*, **18**, 141–153.
6. Allen, A.S., Berkovic, S.F., Cossette, P., Delanty, N., Dlugos, D., Eichler, E.E., Epstein, M.P., Glauser, T., Goldstein, D.B., Han, Y. *et al.* (2013) De novo mutations in epileptic encephalopathies. *Nature*, **501**, 217–221.
7. Veltman, J.A. and Brunner, H.G. (2012) De novo mutations in human genetic disease. *Nat. Rev. Genet.*, **13**, 565–575.
8. Fisher, C.L., Lee, I., Bloyer, S., Bozza, S., Chevalier, J., Dahl, A., Bodner, C., Helgason, C.D., Hess, J.L., Humphries, R.K. *et al.* (2010) Additional sex combs-like 1 belongs to the enhancer

of trithorax and polycomb group and genetically interacts with Cbx2 in mice. *Dev. Biol.*, **337**, 9–15.
9. Baskind, H.A., Na, L., Ma, Q., Patel, M.P., Geenen, D.L. and Wang, Q.T. (2009) Functional conservation of Asxl2, a murine homolog for the Drosophila enhancer of trithorax and polycomb group gene Asx. *PLoS One*, **4**, e4750.
10. Gaytán de Ayala Alonso, A., Gutiérrez, L., Fritsch, C., Papp, B., Beuchle, D. and Müller, J. (2007) A genetic screen identifies novel polycomb group genes in Drosophila. *Genetics*, **176**, 2099–2108.
11. Katoh, M. (2013) Functional and cancer genomics of ASXL family members. *Br. J. Cancer*, **109**, 299–306.
12. Aravind, L. and Iyer, L.M. (2012) The HARE-HTH and associated domains: novel modules in the coordination of epigenetic DNA and protein modifications. *Cell Cycle*, **11**, 119–131.
13. Fisher, C.L., Randazzo, F., Humphries, R.K. and Brock, H.W. (2006) Characterization of Asxl1, a murine homolog of Additional sex combs, and analysis of the Asx-like gene family. *Gene*, **369**, 109–118.
14. Gelsi-Boyer, V., Brecqueville, M., Devillier, R., Murati, A., Mozziconacci, M.J. and Birnbaum, D. (2012) Mutations in ASXL1 are associated with poor prognosis across the spectrum of malignant myeloid diseases. *J. Hematol. Oncol.*, **5**, 12.
15. Katoh, M. (2015) Functional proteomics of the epigenetic regulators ASXL1, ASXL2 and ASXL3: a convergence of proteomics and epigenetics for translational medicine. *Expert. Rev. Proteomics.*, **12**, 317–328.
16. Di Croce, L. and Helin, K. (2013) Transcriptional regulation by Polycomb group proteins. *Nat. Struct. Mol. Biol.*, **20**, 1147–1155.
17. Scheuermann, J.C., de Ayala Alonso, A.G., Oktaba, K., Ly-Hartig, N., McGinty, R.K., Fraterman, S., Wilm, M., Muir, T.W. and Müller, J. (2010) Histone H2A deubiquitinase activity of the Polycomb repressive complex PR-DUB. *Nature*, **465**, 243–247.
18. Lai, H.L. and Wang, Q.T. (2013) Additional sex combs-like 2 is required for polycomb repressive complex 2 binding at select targets. *PLoS One*, **8**, e73983.
19. Gao, Z., Lee, P., Stafford, J.M., von Schimmelmann, M., Schaefer, A. and Reinberg, D. (2014) An AUTS2-Polycomb complex activates gene expression in the CNS. *Nature*, **516**, 349–354.
20. Awad, S., Al-Dosari, M.S., Al-Yacoub, N., Colak, D., Salih, M.A., Alkuraya, F.S. and Poizat, C. (2013) Mutation in PHC1 implicates chromatin remodeling in primary microcephaly pathogenesis. *Hum. Mol. Genet.*, **22**, 2200–2213.
21. Cho, Y.S., Kim, E.J., Park, U.H., Sin, H.S. and Um, S.J. (2006) Additional sex comb-like 1 (ASXL1), in cooperation with SRC-1, acts as a ligand-dependent coactivator for retinoic acid receptor. *J. Biol. Chem.*, **281**, 17588–17598.
22. Abdel-Wahab, O., Adli, M., LaFave, L.M., Gao, J., Hricik, T., Shih, A.H., Pandey, S., Patel, J.P., Chung, Y.R., Koche, R. *et al.* (2012) ASXL1 mutations promote myeloid transformation through loss of PRC2-mediated gene repression. *Cancer Cell*, **22**, 180–193.
23. Chi, P., Allis, C.D. and Wang, G.G. (2010) Covalent histone modifications—miswritten, misinterpreted and mis-erased in human cancers. *Nat. Rev. Cancer*, **10**, 457–469.
24. Sanchez, R. and Zhou, M.M. (2011) The PHD finger: a versatile epigenome reader. *Trends Biochem. Sci.*, **36**, 364–372.
25. Endoh, M., Endo, T.A., Endoh, T., Isono, K., Sharif, J., Ohara, O., Toyoda, T., Ito, T., Eskeland, R., Bickmore, W.A. *et al.* (2012) Histone H2A mono-ubiquitination is a crucial step to mediate PRC1-dependent repression of developmental genes to maintain ES cell identity. *PLoS Genet.*, **8**, e1002774.
26. Wang, H., Wang, L., Erdjument-Bromage, H., Vidal, M., Tempst, P., Jones, R.S. and Zhang, Y. (2004) Role of histone H2A ubiquitination in Polycomb silencing. *Nature*, **431**, 873–878.
27. Stock, J.K., Giadrossi, S., Casanova, M., Brookes, E., Vidal, M., Koseki, H., Brockdorff, N., Fisher, A.G. and Pombo, A. (2007) Ring1-mediated ubiquitination of H2A restrains poised RNA polymerase II at bivalent genes in mouse ES cells. *Nat. Cell. Biol.*, **9**, 1428–1435.
28. Inoue, D., Kitaura, J., Togami, K., Nishimura, K., Enomoto, Y., Uchida, T., Kagiyama, Y., Kawabata, K.C., Nakahara, F., Izawa, K. *et al.* (2013) Myelodysplastic syndromes are induced by histone methylation–altering ASXL1 mutations. *J. Clin. Invest.*, **123**, 4627–4640.
29. Abdel-Wahab, O., Gao, J., Adli, M., Dey, A., Trimarchi, T., Chung, Y.R., Kuscu, C., Hricik, T., Ndiaye-Lobry, D., Lafave, L.M. *et al.* (2013) Deletion of Asxl1 results in myelodysplasia and severe developmental defects in vivo. *J. Exp. Med.*, **210**, 2641–2659.
30. Soto, M.C., Chou, T.B. and Bender, W. (1995) Comparison of germline mosaics of genes in the Polycomb group of Drosophila melanogaster. *Genetics*, **140**, 231–243.
31. Ashburner, M. and Lewis, S. (2002) On ontologies for biologists: the Gene Ontology—untangling the web. *Novartis. Found. Symp.*, **247**, 66–80; discussion 80–63, 84–90, 244–252.
32. Alexa, A., Rahnenführer, J. and Lengauer, T. (2006) Improved scoring of functional groups from gene expression data by decorrelating GO graph structure. *Bioinformatics*, **22**, 1600–1607.
33. Harris, M.A., Clark, J., Ireland, A., Lomax, J., Ashburner, M., Foulger, R., Eilbeck, K., Lewis, S., Marshall, B., Mungall, C. *et al.* (2004) The Gene Ontology (GO) database and informatics resource. *Nucleic Acids Res.*, **32**, D258–D261.
34. Draghici, S., Khatri, P., Tarca, A.L., Amin, K., Done, A., Voichita, C., Georgescu, C. and Romero, R. (2007) A systems biology approach for pathway level analysis. *Genome Res.*, **17**, 1537–1545.
35. Khatri, P., Voichita, C., Kattan, K., Ansari, N., Khatri, A., Georgescu, C., Tarca, A.L. and Draghici, S. (2007) Onto-Tools: new additions and improvements in 2006. *Nucleic Acids Res.*, **35**, W206–W211.
36. Tarca, A.L., Draghici, S. and Romero, R. (2009) Developing classifiers for the detection of cancer using multi-analytes. *Methods Mol. Biol.*, **520**, 259–272.
37. Kanehisa, M. and Goto, S. (2000) KEGG: kyoto encyclopedia of genes and genomes. *Nucleic Acids Res.*, **28**, 27–30.
38. Kanehisa, M., Goto, S., Sato, Y., Furumichi, M. and Tanabe, M. (2012) KEGG for integration and interpretation of large-scale molecular data sets. *Nucleic Acids Res.*, **40**, D109–D114.
39. Kanehisa, M., Goto, S., Sato, Y., Kawashima, M., Furumichi, M. and Tanabe, M. (2014) Data, information, knowledge and principle: back to metabolism in KEGG. *Nucleic Acids Res.*, **42**, D199–D205.
40. Lindhurst, M.J., Sapp, J.C., Teer, J.K., Johnston, J.J., Finn, E.M., Peters, K., Turner, J., Cannons, J.L., Bick, D., Blakemore, L. *et al.* (2011) A mosaic activating mutation in AKT1 associated with the Proteus syndrome. *N. Engl. J. Med.*, **365**, 611–619.
41. Acuna-Hidalgo, R., Bo, T., Kwint, M.P., van de Vorst, M., Pinelli, M., Veltman, J.A., Hoischen, A., Vissers, L.E. and Gilissen, C. (2015) Post-zygotic point mutations are an underrecognized source of de novo genomic variation. *Am. J. Hum. Genet.*, **97**, 67–74.
42. Gelsi-Boyer, V., Trouplin, V., Adélaïde, J., Bonansea, J., Cervera, N., Carbuccia, N., Lagarde, A., Prebet, T., Nezri, M., Sainty, D. *et al.* (2009) Mutations of polycomb-associated gene ASXL1 in myelodysplastic syndromes and chronic myelomonocytic leukaemia. *Br. J. Haematol.*, **145**, 788–800.

43. Micol, J.B., Duployez, N., Boissel, N., Petit, A., Geffroy, S., Nibourel, O., Lacombe, C., Lapillonne, H., Etancelin, P., Figeac, M. *et al.* (2014) Frequent ASXL2 mutations in acute myeloid leukemia patients with t(8;21)/RUNX1-RUNX1T1 chromosomal translocations. *Blood*, **124**, 1445–1449.
44. Stephens, P.J., Tarpey, P.S., Davies, H., Van Loo, P., Greenman, C., Wedge, D.C., Nik-Zainal, S., Martin, S., Varela, I., Bignell, G. R. *et al.* (2012) The landscape of cancer genes and mutational processes in breast cancer. *Nature*, **486**, 400–404.
45. Grasso, C.S., Wu, Y.M., Robinson, D.R., Cao, X., Dhanasekaran, S.M., Khan, A.P., Quist, M.J., Jing, X., Lonigro, R.J., Brenner, J.C. *et al.* (2012) The mutational landscape of lethal castration-resistant prostate cancer. *Nature*, **487**, 239–243.
46. Williams, D.S., Bird, M.J., Jorissen, R.N., Yu, Y.L., Walker, F., Zhang, H.H., Nice, E.C. and Burgess, A.W. (2010) Nonsense mediated decay resistant mutations are a source of expressed mutant proteins in colon cancer cell lines with microsatellite instability. *PLoS One*, **5**, e16012.
47. Huether, R., Dong, L., Chen, X., Wu, G., Parker, M., Wei, L., Ma, J., Edmonson, M.N., Hedlund, E.K., Rusch, M.C. *et al.* (2014) The landscape of somatic mutations in epigenetic regulators across 1,000 paediatric cancer genomes. *Nat. Commun.*, **5**, 3630.
48. Stransky, N., Egloff, A.M., Tward, A.D., Kostic, A.D., Cibulskis, K., Sivachenko, A., Kryukov, G.V., Lawrence, M.S., Sougnez, C., McKenna, A. *et al.* (2011) The mutational landscape of head and neck squamous cell carcinoma. *Science*, **333**, 1157–1160.
49. Li, M., Zhao, H., Zhang, X., Wood, L.D., Anders, R.A., Choti, M.A., Pawlik, T.M., Daniel, H.D., Kannangai, R., Offerhaus, G.J. *et al.* (2011) Inactivating mutations of the chromatin remodeling gene ARID2 in hepatocellular carcinoma. *Nat. Genet.*, **43**, 828–829.
50. Balbás-Martínez, C., Sagrera, A., Carrillo-de-Santa-Pau, E., Earl, J., Márquez, M., Vazquez, M., Lapi, E., Castro-Giner, F., Beltran, S., Bayés, M. *et al.* (2013) Recurrent inactivation of STAG2 in bladder cancer is not associated with aneuploidy. *Nat. Genet.*, **45**, 1464–1469.
51. Berger, M.F., Hodis, E., Heffernan, T.P., Deribe, Y.L., Lawrence, M.S., Protopopov, A., Ivanova, E., Watson, I.R., Nickerson, E., Ghosh, P. *et al.* (2012) Melanoma genome sequencing reveals frequent PREX2 mutations. *Nature*, **485**, 502–506.
52. Jones, S., Zhang, X., Parsons, D.W., Lin, J.C., Leary, R.J., Angenendt, P., Mankoo, P., Carter, H., Kamiyama, H., Jimeno, A. *et al.* (2008) Core signaling pathways in human pancreatic cancers revealed by global genomic analyses. *Science*, **321**, 1801–1806.
53. Bravo, G.M., Lee, E., Merchan, B., Kantarjian, H.M. and García-Manero, G. (2014) Integrating genetics and epigenetics in myelodysplastic syndromes: advances in pathogenesis and disease evolution. *Br. J. Haematol.*, **166**, 646–659.
54. Mehdipour, P., Santoro, F. and Minucci, S. (2015) Epigenetic alterations in acute myeloid leukemias. *FEBS J.*, **282**, 1786–1800.
55. Shih, A.H., Abdel-Wahab, O., Patel, J.P. and Levine, R.L. (2012) The role of mutations in epigenetic regulators in myeloid malignancies. *Nat. Rev. Cancer*, **12**, 599–612.
56. Cazzola, M., Della Porta, M.G. and Malcovati, L. (2013) The genetic basis of myelodysplasia and its clinical relevance. *Blood*, **122**, 4021–4034.
57. Duployez, N., Micol, J.B., Boissel, N., Petit, A., Geffroy, S., Bucci, M., Lapillonne, H., Renneville, A., Leverger, G., Ifrah, N. *et al.* (2015) Unlike ASXL1 and ASXL2 mutations, ASXL3 mutations are rare events in acute myeloid leukemia with t(8;21). *Leuk. Lymphoma*, 1–2, doi: 10.3109/10428194.2015.1037754.
58. Beunders, G., Voorhoeve, E., Golzio, C., Pardo, L.M., Rosenfeld, J.A., Talkowski, M.E., Simonic, I., Lionel, A.C., Vergult, S., Pyatt, R.E. *et al.* (2013) Exonic deletions in AUTS2 cause a syndromic form of intellectual disability and suggest a critical role for the C terminus. *Am. J. Hum. Genet.*, **92**, 210–220.
59. Nagamani, S.C., Erez, A., Ben-Zeev, B., Frydman, M., Winter, S., Zeller, R., El-Khechen, D., Escobar, L., Stankiewicz, P., Patel, A. *et al.* (2013) Detection of copy-number variation in AUTS2 gene by targeted exonic array CGH in patients with developmental delay and autistic spectrum disorders. *Eur. J. Hum. Genet.*, **21**, 343–346.
60. Adorno, M., Sikandar, S., Mitra, S.S., Kuo, A., Nicolis Di Robilant, B., Haro-Acosta, V., Ouadah, Y., Quarta, M., Rodriguez, J., Qian, D. *et al.* (2013) Usp16 contributes to somatic stem-cell defects in Down's syndrome. *Nature*, **501**, 380–384.
61. Yang, W., Lee, Y.H., Jones, A.E., Woolnough, J.L., Zhou, D., Dai, Q., Wu, Q., Giles, K.E., Townes, T.M. and Wang, H. (2014) The histone H2A deubiquitinase Usp16 regulates embryonic stem cell gene expression and lineage commitment. *Nat. Commun.*, **5**, 3818.
62. Jacobs, J.J., Kieboom, K., Marino, S., DePinho, R.A. and van Lohuizen, M. (1999) The oncogene and Polycomb-group gene bmi-1 regulates cell proliferation and senescence through the ink4a locus. *Nature*, **397**, 164–168.
63. Pemberton, H., Anderton, E., Patel, H., Brookes, S., Chandler, H., Palermo, R., Stock, J., Rodriguez-Niedenführ, M., Racek, T., de Breed, L. *et al.* (2014) Genome-wide co-localization of Polycomb orthologs and their effects on gene expression in human fibroblasts. *Genome Biol.*, **15**, R23.
64. Liu, Y., Sanoff, H.K., Cho, H., Burd, C.E., Torrice, C., Ibrahim, J. G., Thomas, N.E. and Sharpless, N.E. (2009) Expression of p16 (INK4a) in peripheral blood T-cells is a biomarker of human aging. *Aging Cell*, **8**, 439–448.
65. Janzen, V., Forkert, R., Fleming, H.E., Saito, Y., Waring, M.T., Dombkowski, D.M., Cheng, T., DePinho, R.A., Sharpless, N.E. and Scadden, D.T. (2006) Stem-cell ageing modified by the cyclin-dependent kinase inhibitor p16INK4a. *Nature*, **443**, 421–426.
66. Wu, X., Johansen, J.V. and Helin, K. (2013) Fbxl10/Kdm2b recruits polycomb repressive complex 1 to CpG islands and regulates H2A ubiquitylation. *Mol. Cell*, **49**, 1134–1146.
67. Quinonez, S.C. and Innis, J.W. (2014) Human HOX gene disorders. *Mol. Genet. Metab.*, **111**, 4–15.
68. Villegas, J. and McPhaul, M. (2005) Establishment and culture of human skin fibroblasts. *Curr. Protoc. Mol. Biol.*, Chapter 28, Unit 28.23.
69. Trapnell, C., Pachter, L. and Salzberg, S.L. (2009) TopHat: discovering splice junctions with RNA-Seq. *Bioinformatics*, **25**, 1105–1111.
70. Kim, D. and Salzberg, S.L. (2011) TopHat-Fusion: an algorithm for discovery of novel fusion transcripts. *Genome Biol.*, **12**, R72.
71. Love, M.I., Huber, W. and Anders, S. (2014) Moderated estimation of fold change and dispersion for RNA-seq data with DESeq2. *Genome Biol.*, **15**, 550.
72. Picelli, S., Björklund, A.K., Reinius, B., Sagasser, S., Winberg, G. and Sandberg, R. (2014) Tn5 transposase and tagmentation procedures for massively scaled sequencing projects. *Genome Res.*, **24**, 2033–2040.
73. Detilleux, P.G., Deyoe, B.L. and Cheville, N.F. (1990) Penetration and intracellular growth of Brucella abortus in nonphagocytic cells in vitro. *Infect. Immun.*, **58**, 2320–2328.
74. Li, H. and Durbin, R. (2009) Fast and accurate short read alignment with Burrows-Wheeler transform. *Bioinformatics*, **25**, 1754–1760.